Numerical Investigation of the Thermo-flow Processes in an Automobile Underhood

JM van Zyl[a], TM Harms[b] and AB Taylor[c]
Received 12 June 2008, in revised form xx November 2009 and accepted xx November 2009

South Africa currently manufactures and assembles many vehicles for both local and export markets. Recent events have indicated that South Africa may increase its involvement in the research and development of these vehicles and would be required to contribute to engineering tools needed therefore. One aspect of vehicle design is thermal management systems, which require tools including computational fluid dynamic models to simulate the flow and thermal processes that occur in and around the vehicle. Described here is an experimental and numerical investigation of a 1996 model Volkswagen Citi Golf underhood environment. Two cases were investigated both experimentally and numerically. The first assumed the radiator-cooling fan produced all the airflow through the underhood and the second used the large subsonic wind tunnel at Stellenbosch University to provide a constant airflow. The experimental and numerical results indicated that even with simplistic geometries of complex environments like the underhood, the flow and thermal patterns predicted by numerical simulations compared acceptably to measured experimental data.

Additional Keywords: radiator, temperature, porous resistance, heat transfer

Nomenclature

Roman

b	Thickness	[m]
c_p	Constant-pressure specific heat	[J/kg K]
F	Diffusional thermal energy flux	[N/m s]
g	Gravitational acceleration	[m/s^2]
k	Turbulent kinetic energy	[m^2/s^2]
p	Piezometric pressure	[N/m^2]
r	Radius	[m]
s	Source term	
T	Temperature	[K]
t	Time	[s]
u	Velocity	[m/s]
x	Cartesian coordinate	[m]

Greek

α	Porous inertial resistance	[kg/m^4]
β	Porous viscous resistance	[kg/m^3 s]
ε	Turbulent dissipation rate	[m^2/s^3]
ρ	Density	[kg/m^3]
τ	Stress tensor	[N/m^2]

Subscripts

0	Reference
eq	Equivalent
env	Environment
h	Heat
i, j	Indices
m	Datum
mag	Magnitude
rad	Radiator
t	Thermal

Superscripts

$\bar{}$	Mean
0	Reference

Abbreviations

CFD	Computational fluid dynamics
CAD	Computer aided design
CAE	Computer aided engineering

1. Introduction

Development and application of commercial computational fluid dynamics (CFD) software packages along with increased computing capabilities have allowed engineers and designers enhanced abilities to investigate complex fluid and thermal problems. CFD involves numerically solving the governing fluid and thermodynamic equations describing flow of fluids using a discretised domain.

The automotive industry is increasingly implementing CFD as a design and analysis tool, continuously improving its vehicles. These include reducing underhood thermal conditions and emissions, improving performance, increasing safety and optimising the driver's perception of comfort. International automotive companies are currently using CFD to design various vehicle aspects including climate control, underhood thermal management, engine performance and aerodynamics. A more specialised and better-known field is automotive racing such as F1 and Le Mans, where every aspect involving fluid flow, combustion and heat transfer are meticulously investigated using CFD to optimise performance from each vehicle.

Literature revealed various experimental and numerical investigations conducted to analyse and improve vehicle design. These include determining the best options for reducing temperatures within the underhood[1], experimentally measuring wake profiles of automotive cooling fans[2], analysing catalytic converters with CFD[3] and

a Graduate Student, Department of Mechanical and Mechatronic Engineering, University of Stellenbosch, Private Bag X1, Matieland, South Africa. E-mail: jmvz@sun.ac.za
b Department of Mechanical and Mechatronic Engineering, University of Stellenbosch, MSAIMechE.
c Managing Director, Cape Advanced Engineering (Pty) Ltd. MSAIMechE. http://organergy.co.za

development of numerical fan models to reduce computing requirements[4].

Pressure to convert from experimental based engineering to simulation-based engineering[5] is driving the automotive industry to design and optimise their vehicles using computer aided design (CAD) packages and computer aided engineering (CAE) software such as CFD. As South Africa is involved with manufacturing and assembling vehicles for international motorcar companies including Toyota and Volkswagen, its automotive industry is developing a need for CFD models to assist with modification of these vehicles to improve them for local and international application.

Forming part of this process initiative, it was conceived to develop a simplified model of one of the highly successful vehicles in South Africa, namely the 1.3 litre Volkswagen Citi Golf, and investigate the airflow within its underhood environment using the commercial CFD package STAR-CCM+ (CD-Adapco). It includes the use of simplified models to simulate effects from the cooling fan and radiator and comparison of experimental and numerical results. The objective was to develop a platform from which further research and development could develop. Typical long-term design objectives may include minimising unnecessary energy waste or optimising engine warm up time for better efficiency and reduced wear.

2. Materials and Methods

2.1 Experimental

Experimental measurements provided information for the CFD boundary conditions and numerical verification. Tests were conducted at the Department of Mechanical and Mechatronic Engineering at the University of Stellenbosch using its large 373 kW subsonic wind tunnel. A 1996 model 1.3 litre Volkswagen Citi Golf was selected as this vehicle and similar models are of the most successful in South Africa and has proven itself for many years.

Wind tunnel tests required the vehicle be parked upon a custom-built ramp[6] and experience both near stagnant surrounding air and airflow of 5 m/s drawn over the vehicle to evaluate conditions of the vehicle idling in no-wind and low-wind conditions respectively. The cooling-fan remained permanently enabled during the stagnant case to provide airflow through the radiator and disabled during the low-wind case as the wind tunnel provided the airflow.

T-Type Thermocouples measured the temperatures of the air in the four corners of the underhood, in and out of the radiator and fan and the surface temperature of the engine block. Figure 1 and table 1 present the thermocouples positions within the underhood. A TI-30 ThermoView thermal imager from Raytek measured the surface temperatures of the exhaust manifold, gearbox, radiator and overflow reservoir.

A digital TA 5 hand-held hot-film anemometer from DP Measurement confirmed the airspeed through the tunnel and measured the air speed through the cooling-fan prior to data capturing as not to interfere with experimental readings. The airspeed through the wind tunnel was verified by measuring the velocities at the four corners and centre of the tunnel. These readings indicated that the inlet conditions remained approximately uniform.

Figure 1: Thermocouple positions in the underhood

Position	Description
1	Ambient Air
2	Front left corner
3	Back left corner
4	Engine surface
5	Radiator inlet
6	Radiator outlet
7	Fan outlet
8	Back right corner
9	Front right corner

Table 1: Description of thermocouple positions

Air speed measurements were taking at arbitrary locations at the fan outlet and used to determine the peak flow velocity through the fan. A Pitot static probe (figure 2) positioned in front on the vehicle measured the incoming wind tunnel air speed during data capturing. The probe function was to ensure that the airflow through the wind tunnel remain within an acceptable constraint of 10 % during the 5 m/s tests.

Heat transfer coefficient and porous resistance of the radiator were determined separately at various airflow rates using the heat exchanger test facility situated at the Department of Mechanical and Mechatronic Engineering of Stellenbosch University.

Figure 2: Pitot static probe position relative to vehicle

A differential pressure transducer measured the pressure drop while the heat transfer was determined by measuring the hot water mass flow rate along with inlet and outlet water temperatures. Airflow through the radiator was varied using a frequency control to adjust the centrifugal fan speed of the test facility. Porous resistance and heat transfer coefficients were related to air speed through the radiator and fitted with polynomials as presented in figures 3 and 4. These curves were used to model the radiator in the numerical investigations.

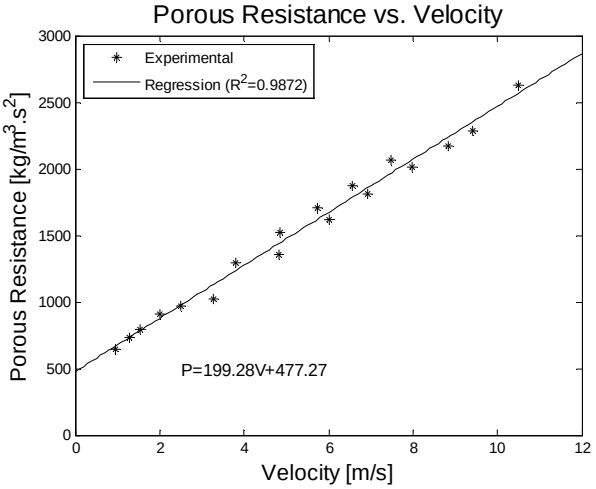

Figure 3: Porous resistance versus velocity result from radiator tests

2.2 Numerical model and investigation

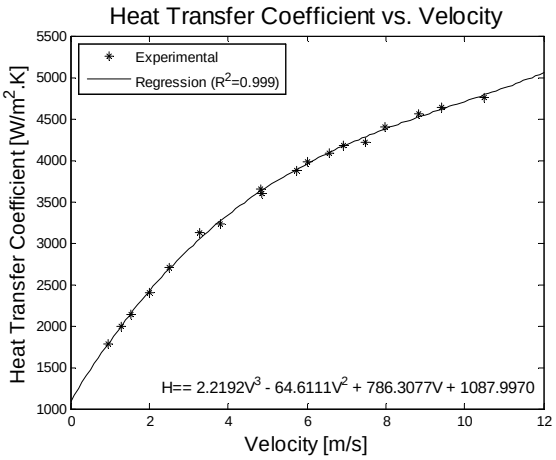

Figure 4: Heat transfer versus velocity result from the radiator tests

The complex underhood component geometries were simplified and excluded unnecessary modelling complications including piping and electric wiring throughout the underhood domain. This simplified geometry of the Volkswagen Citi Golf was created with Solid Edge, version 14 from EDS PLC Solutions. Figure 5 shows a top view of the underhood region with the bonnet removed.

STAR-Design version 4.02 from CD-Adapco was used to prepare the CAD geometry for volume discretisation.

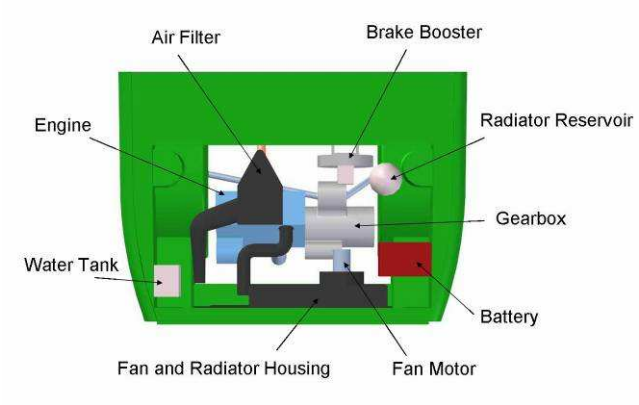

Figure 5: Top view of the Volkswagen Citi Golf underhood model

The vehicle geometry presented by the wire frame model in figure 6 was imported into this package and used to create a solid volume representation of the air within the underhood and around the vehicle, with the block surrounding the vehicle representing the wind tunnel. STAR-Design was further used to generate a surface mesh from the solid volume, which was imported into STAR-CCM+ version 4.02, with which the air volume was discretised using polyhedral cells and numerical simulations were conducted.

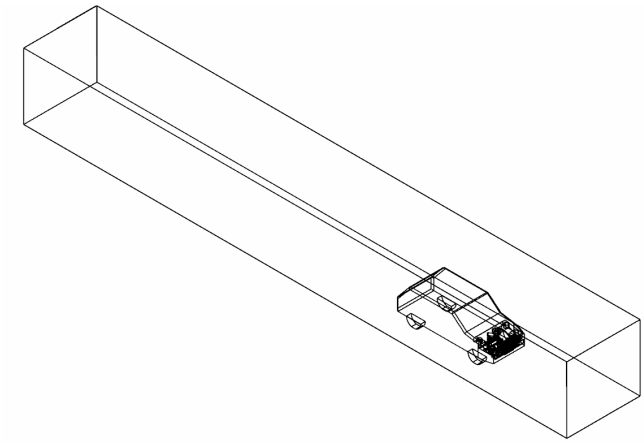

Figure 6: Wire frame of volume used for grid generation

Inlet and outlet boundary conditions included a prescribed mass flow rate applied to the tunnel exit (behind the vehicle) and a specified inlet pressure applied to the tunnel inlet (front of vehicle). The prescribed mass flow rate boundary applied to the tunnel exit captured effects of the wind tunnel fan drawing the air over the vehicle and out the tunnel instead of blowing it into the tunnel and over the vehicle. This boundary was positioned a suitable distance downstream from the vehicle to remain outside the wake of the vehicle and avoid numerical error propagating into the upstream airflow. Fixed surface temperatures were assigned to heat source surfaces within the underhood including the engine, radiator reservoir, gearbox, hot water pipe, exhaust manifold and heat exchanger as illustrated in figure 7. All remaining surfaces were modelled as adiabatic including the bonnet and tunnel walls.

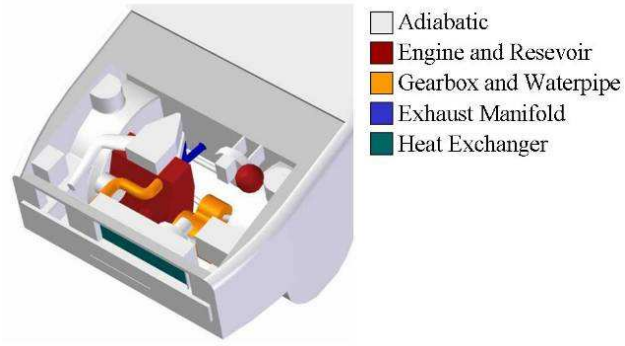

Figure 7: Surfaces with fixed temperatures

Table 2 provides the boundary types and conditions applied to the model. The mass flow for the wind tunnel off case was prescribed a non-zero value to provide stability to the numerical simulations. A zero mass flow condition through the tunnel allows numerical error to prescribe the airflow, which caused unrealistic results. The mass flow rates of 5.12 kg/s and 51.21 kg/s through the tunnel correlates to airflow velocities of 0.5 m/s and 5 m/s respectively.

Internal models included the momentum and energy equations, High-Reynolds number *k-ε* turbulence model with standard wall functions (law-of-the-wall)[7] and buoyancy. At the time this project was undertaken, the computing power available was limited and for this reason radiation and near wall investigations were not included in the simulations, as their calculations are highly computer intensive. The effects of radiation were considered negligible for the purpose of this study, as the interest was only the airflow through the underhood upon which radiation had little effect. Radiation from components such as the exhaust manifold and pipe will affect exposed surfaces including critical underhood components, but these investigations were outside the scope of this study. Using the exhaust pipe as the worst-case scenario, the heat flux was calculated as follows:

$$\begin{aligned}\dot{Q} &= \sigma A(T_{exh}^4 - T_{sur}^4) \\ &= 5.67\times10^{-8}\times0.094\times(513^4 - 313^4) \\ &= 317.976 \text{ W}\end{aligned}$$

while the heat flux added to the air by the radiator was well over 11 kW.

Internal equations used by CFD software include the Navier-Stokes equation:

$$\frac{\partial \rho u_i}{\partial t} + \frac{\partial}{\partial x_j}\left(\rho u_j u_i - \tau_{ij}\right) = -\frac{\partial p}{\partial x_i} + s_i \quad (1)$$

Here static pressure was adjusted for buoyancy calculations:

$$p = p_s - \rho_0 g_m x_m \quad (2)$$

Fluid enthalpy is calculated from the energy conservation equation:

$$\frac{\partial \rho h_t}{\partial t} + \frac{\partial}{\partial x_j}\left(\rho h_t u_j + F_{h_t,j}\right) = \frac{\partial p}{\partial t} + u_j \frac{\partial p}{\partial x_j} + \tau_{ij}\frac{\partial u_i}{\partial x_j} + s_{i,h} \quad (3)$$

where: $h_t = \bar{c}_p T - c_p^0 T_0$ (4)

Buoyancy was modelled as a momentum source term calculated by:

$$s_{i,b} = g_i\left(\rho - \rho_o\right) \quad (5)$$

Ideal gas law was applied the air to account for density variations due to temperature change.

$$\rho = \frac{P}{RT} \quad (6)$$

The cooling fan was modelled using the actual fan geometry and moving reference frames. Moving reference frames allow a steady state simulation to capture the effects of a moving object at any point of time. Although this does not capture the unsteady nature of the fan, it was sufficient for the purpose of this study.

The radiator effects were modelled using experimentally determined porous resistance and energy source terms as described earlier. Thus, as the air flowed through the radiator it loss momentum and added energy to the air causing it to rise in temperature. The porous resistance was modelled using with the following correlation:

$$s_{i,rad} = \left(\alpha u_{mag} + \beta\right)u_i \quad (7)$$

with α =199.28 kg/m^4 and β =477.27 kg/m^{3}s obtained from figure 3.

The heat transfer was calculated using an overall heat transfer co-efficient *H* calculated from the correlation shown

Component or Position	Wind tunnel off		Wind tunnel on	
	Boundary Type	Properties	Boundary Type	Properties
Engine Surface	Non-slip Wall	353.15 K	Non-slip Wall	357.15 K
Gearbox Surface	Non-slip Wall	333.15 K	Non-slip Wall	333.15 K
Exhaust Manifold Surface	Non-slip Wall	495.15 K	Non-slip Wall	511.15 K
Hot Water Pipe	Non-slip Wall	333.15 K	Non-slip Wall	333.15 K
Water Reservoir	Non-slip Wall	353.15 K	Non-slip Wall	357.15 K
Tunnel Wall Surface	Non-slip Wall	298.15 K	Non-slip Wall	298.15 K
Tunnel Entrance	Pressure	101 325 Pa	Pressure	101 325 Pa
Tunnel Exit	Mass flow	-5.12 kg/s	Mass flow	-51.21 kg/s

Table 2: Boundary conditions applied to the simulations

in figure 4 by dividing the heat transferred by the temperature difference between the radiator and surrounding air and the total radiator frontal face area.

$$s_{i,h} = \frac{H\left(T_{rad} - T_{env}\right)}{b_{rad}} \quad (8)$$

where:

$$H = 2.219u_i^3\text{-}64.611u_i^2\text{+}786.3u_i\text{+}1087.997 \ \text{W/m}^2\text{K} \quad (9)$$

Table 3 presents the remaining simulation parameters used during the numerical investigations.

Description	Value
Inlet turbulence intensity	1%
Inlet turbulent length scale	0.02 m
Inlet air temperature	296.65 K
Implicit solver Courant number	10.0
Turbulent under-relaxation	0.8
Turbulent viscosity under-relaxation	1.0
Dynamic viscosity of air	1.855×10^{-5} Pa·s
Specific heat of air	1007 J/kg·K
Thermal conductivity of air	0.02603 W/m·K
Air reference density for buoyancy calculations	1.18 kg/m^3
Turbulent Prandtl number	0.9
Discretisation scheme	Second order upwind
Gravity	9.81 m/s^2

Table 3: Additional simulation parameters

4. Results

4.1 Experimental results

The two experimental cases investigated were the vehicle idling in wind speeds of 0 m/s and 5 m/s respectively.

The temperatures of the air at the designated locations indicated in figure 1 were measured using thermocouples, while the thermal imager measured the surface temperatures of the exhaust manifold, water reservoir and radiator. Table 4 provides the averaged temperatures measured.

Two extremes were observed from the experimental results. For the case where the radiator cooling-fan produced all the airflow, underhood temperatures averaged around 313.15 K and the temperatures of the air surrounding the radiator averaged around 309.15 K. This was attributed to the warm air from the radiator being blown into the underhood environment and further heated by the engine and exhaust manifold. For the case where the wind tunnel produced all the airflow, the underhood temperatures ranged between 296.15 K and 306.15 K, with radiator air temperatures between 337.15 K and 346.15 K. It is clear that although the underhood environment is cooled more effectively by surrounding air in this case, the near stationary air around the radiator causes its efficiency to decrease hence resulting in high engine and exhaust manifold temperatures.

This indicates the worst-case scenario for electrical components occurs when the radiator-cooling fan solely produces the airflow.

Position	Wind tunnel off [K]	Wind tunnel on [K]
Ambient Air	296.87 ± 1.08	296.46 ± 0.49
Front Right	312.42 ± 0.73	297.58 ± 0.46
Back Right	314.90 ± 0.83	302.28 ± 1.12
Front Left	313.62 ± 0.78	297.71 ± 0.87
Back Left	314.15 ± 0.95	306.36 ± 1.59
Radiator Inlet	297.74 ± 1.73	300.79 ± 5.77
Radiator Outlet	309.08 ± 0.84	345.59 ± 1.27
Fan Outlet	310.28 ± 2.71	337.33 ± 2.02
Engine Surface	353.27 ± 0.69	357.24 ± 0.46
Exhaust Pipe	495.15	511.15
Radiator	298.15 – 333.15	347.15

Table 4: Measured underhood temperatures

The hand-held hot film anemometer was used to determine airspeed in both test cases. For the case where the wind tunnel was switched off and the radiator cooling-fan produced all the airflow, the fan peak air speed was measured at approximately 13 m/s. For the case where the wind tunnel was activated and cooling-fan remaining disabled, the wind tunnel air speed was measured at 5.19 ± 0.31 m/s. The later airflow through the wind tunnel caused a low pressure zone within the underhood, drawing air in through and grill and extracting the warm air from underneath the underhood causing lower temperatures mentioned above.

4.2 Numerical results

The numerical results were evaluated in terms of the convergence of each simulation, its grid independence and y^+ values. Convergence of the solutions was evaluated using normalised residuals and field values from the solution. Thus while the residuals decrease, the solution approached a single converged solution. Ideally, the residuals should decrease to zero once the solution has converged to a solution. This is not possible, as numerical errors restrict the minimum possible residual error and the time required to reach this minimum residual value is usually too long. Thus, simulations are stopped once a specified condition is satisfied. This condition may require residuals to decrease by a predetermined order of magnitude or by specifying a number of iterations. For this study calculations were performed for 10 000 iterations with all residuals decreasing a minimum of 4 orders of magnitude.

A more informative parameter for convergence is field values. Field values are extracted data points from arbitrarily placed positions of interest. Once the values from these points remain constant, the solution is accepted as converged. For this study, temperatures and velocity magnitudes were monitored for convergence.

Grid independence of the solutions was determined by solving the CFD problem on three different grid resolutions and comparing the solutions to each other. The grid resolutions for the three meshes were 398 581 cells, 718 543 cells and 1 226 005 polyhedral cells. Figure 8 provides a sample from the three grids of the velocity profile within the underhood environment. It clearly illustrates that the results obtained from the medium and fine grid resolutions only differ slightly confirming that grid independence was satisfactory.

The applicability of the High Reynolds number *k-ε* turbulence model requires y^+ values to range between 30 and 500. Simulations results were all evaluated to ensure that this condition remained satisfied.

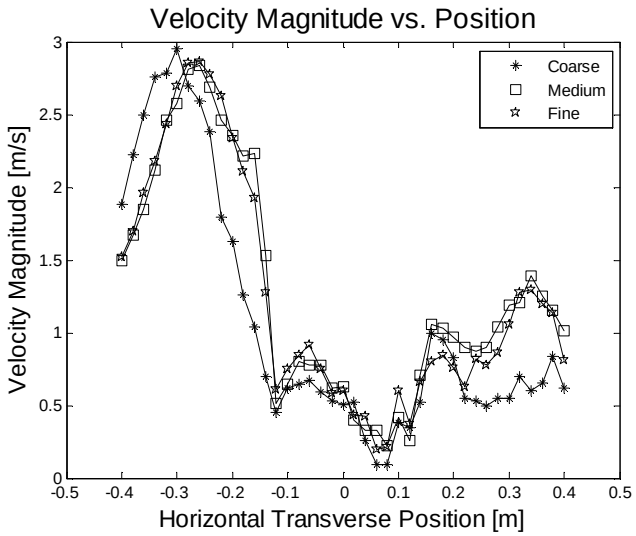

Figure 8: Stationary case velocity magnitude profile within the underhood environment

The numerical results for the case where the radiator-cooling fan produced all the airflow proved to be the worse case scenario. The relative high inlet velocity (13 m/s) through the fan resulted in a warm stream of air, approximately 311.15 K, to enter the underhood. This stream flowed against the back panel of the underhood where it dispersed in all directions losing momentum. The air in the rest of the underhood remained near stationary, allowing other engine components including the engine, exhaust manifold and gearbox to heat the air further as seen in figures 9 and 10.

The case where the radiator-cooling fan remained disabled and the wind tunnel produced the airflow through and over the vehicle at 5 m/s, the airflow through the radiator and fan was significantly reduced to very low speeds, thus the incoming air form the radiator was much warmer than the previous case with temperatures of approximately 343.15 K. The airflow under the vehicle caused a lower pressure to exist beneath the vehicle resulting in air being drawn into the underhood through the grill and out under the vehicle. This extracted warmer air reduced the effects of heating from the engine and exhaust manifold, and drew most of the hot radiator air away from the underhood.

This resulted in an average temperature of approximately 300 K, which is approximately 10 K cooler than the previous case.

4.3 Experimental and numerical comparison

Accuracy of the CFD simulations predicted temperatures throughout the underhood was determined using numerical sensors placed in the model at identical positions as the thermocouples in the experimental tests. These numerical sensors are additional vertices inserted in the CFD mesh, which extracts the interpolated values from the results of the numerical simulations.

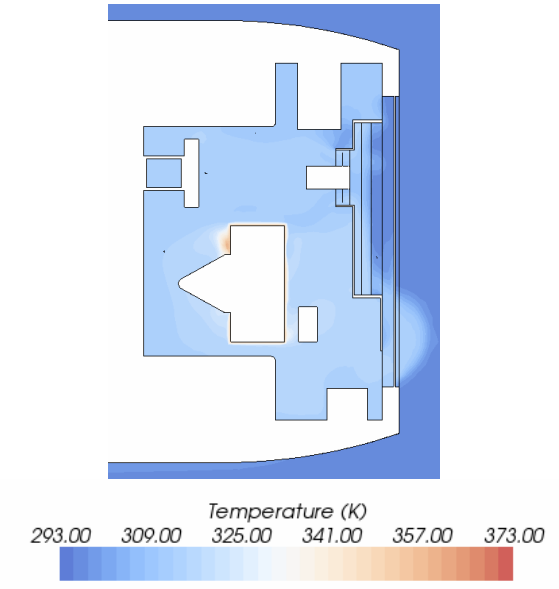

Figure 9: Temperature distribution on a horizontal slice through the under-hood passing through the fan

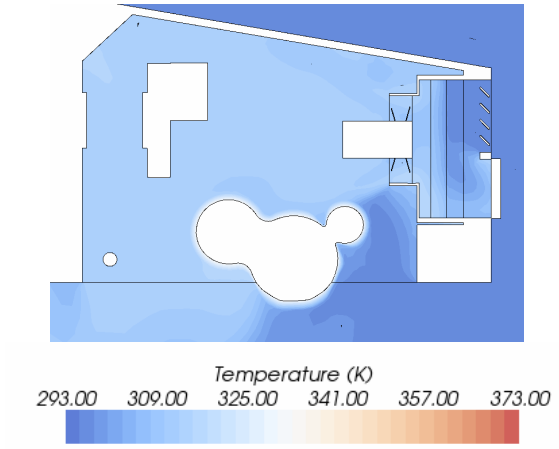

Figure 10: Temperature distribution on a vertical slice through the underhood passing through the fan

Comparing the measured experimental and numerical results for the temperatures, indicate that although the underhood compartment used in the numerical simulations was significantly simplified, with only major components included, the simulations were still capable of predicting the temperatures with an acceptable accuracy of less than 10 % as seen in table 5.

The largest discrepancy found between experimental and numerical temperature readings occur at the back left corner position of the underhood in the stationary case. This difference is attributed to the fan belts and alternator effects, which was not included in the numerical simulations. The fan belts cause air around the back left sensor to be agitated, resulting in better mixing with cooler steams of air thus producing a slightly lower reading in the experimental measurements. The blocks shaded grey were not determine

Position	Wind tunnel off		Wind tunnel on	
	Experimental [K]	Numerical [K]	Experimental [K]	Numerical [K]
Ambient air	296.87 ± 1.08	297.62	296.46 ± 0.49	296.65
Front right	312.42 ± 0.73	311.43	297.58 ± 0.46	296.65
Back right	314.90 ± 0.83	313.21	302.28 ± 1.12	302.7
Front left	313.62 ± 0.78	316.79	297.71 ± 0.87	298.51
Back left	314.15 ± 0.95	316.7	306.36 ± 1.59	308.33
Radiator inlet	297.74 ± 1.73	297.15	300.79 ± 5.77	296.65
Radiator outlet	309.08 ± 0.84	311.87	345.59 ± 1.27	343.53
Fan outlet	310.28 ± 2.71	312.82	337.33 ± 2.02	336.64
Engine zurface	353.27 ± 0.69	353.15	357.24 ± 0.46	357.15
Exhaust pipe	495.15	495.15	511.15	511.15
Radiator	298.15 – 333.15	318.15	347.15	347.15

Table 5: Experimental and numerical comparison

numerically but used as boundary conditions to the numerical simulations to represent the heat sources.

To verify the fan model for the case where the fan produced all the airflow, the experimental and numerical peak readings were compared. The result was that both readings produce approximately 13 m/s indicating that the flow rates produced by the fan were correct. The flow patterns generated by the numerical fan model was visually confirmed by means of tufts that were taped to a Perspex sheet (replacing the bonnet) and the vehicle skirting, which indicated similar swirl effects and flow from out under the vehicle. For the case where the wind tunnel produced all the airflow, the numerical results produced flow patterns as observed in the experimental tests by the tufts.

This indicated that the CFD simulations were capable of predicting the temperature and flow patterns occurring within the underhood, although the geometry was significantly simplified and not all contributing factors included.

5. Conclusion

The experimental measurements produced sufficient information to model the underhood environment of the Volkswagen Citi Golf. Numerical results from the CFD simulation compared well with the experimental data, with all temperature readings falling within 10 % of the measured values. The radiator porous resistance model proved sufficient for numerical modelling and captured all significant effects.

The worst-case scenario was identified as the case where the cooling fan was solely responsible for the cooling of the underhood environment. Temperatures from this condition averaged roughly 313 K, with the engine components playing a major role in heating. Drawing air over the vehicle at 5 m/s resulted in temperatures of approximately 300 K. The high air temperatures of 343 K around the radiator reduced its efficiency. The low airflow through the underhood resulted in elevated exhaust and engine temperatures.

In conclusion, it was determined that CFD could sufficiently model these complex environments using only the major components while remaining within the limited computing power deployed at the time. A platform now exists from which further modelling improvement and research can continue in South Africa.

Acknowledgements

The author grants acknowledgement to the following institutes:

Dr Taylor and Cape Advanced Engineering (Pty) Ltd. for providing the funding and facilities for the project.

Dr Martin van Staden from Aerotherm for the assistance in the use of the STAR-CCM+ CFD software package.

The South African Air Force for the support for funding the licenses for the software package through the Prometheus CFD expertise development project.

References

1. *Winnard D, Venkateswaran G and Barry RE*, Underhood thermal management by controlling airflow, *Society of Automotive Engineers*, 1995, Paper 951013.
2. *Morris SC, Good JJ and Foss JF*, Velocity measurement in the wake of an automotive cooling fan, *Experimental Thermal and Fluid Science*, 1997, 17, 100-106.
3. *Tsinoglou DN, Koltsakis GC, Mirrirlis DK and Yakinthos KJ*, Transient modelling of flow distribution in automotive catalytic converters, *Applied Mathematical Modelling*, 2004, 28, 775–794.
4. *Tzanos CP, and Chien T*, A simple fan model for underhood thermal management analyses, *Society of Automotive Engineering*, 2002, Paper 2002-01-1025.
5. *Shephard MS, Beall MW, O'Bara RM and Webster BE*, Toward Simulation-Based Design, *Finite Elements in Analysis and Design*, 2003, 40, 1575-1598.
6. *Stander JN*, The evaluation of the flow characteristics of a newly installed test ramp, University of Stellenbosch, *Report for vacation training*, 2004.
7. *CD-Adapco*, STAR-CD version 3.24 user methodology manual, 2004, 6-3 – 6-6.